Remote Sensing of Environment xxx (xxxx) xxx–xxx

Contents lists available at ScienceDirect

Remote Sensing of Environment

journal homepage: www.elsevier.com/locate/rse

Identifying the genus or species of individual trees using a three-wavelength airborne lidar system

Brindusa Cristina Budei[a], Benoît St-Onge[b,*], Chris Hopkinson[c], Félix-Antoine Audet[b]

[a] Environmental Sciences Institute, University of Quebec at Montreal, Canada
[b] Department of Geography, University of Quebec at Montreal, Canada
[c] Department of Geography, University of Lethbridge, Canada

ARTICLE INFO

Keywords:
Tree
Species
Genus
Multispectral
Lidar
Intensity
Identification
Random forest
Titan

ABSTRACT

The identification of individual tree species is crucial for forest inventory, carbon stocks assessment as well as for habitat and ecosystem change studies. Previous studies have shown the potential of using both the geometrical information (proportions, shape of the crown profile, etc.) and return intensities of airborne laser scanning (ALS) point clouds to identify trees. So far, single wavelength (1064 nm or 1550 nm) ALS systems have been the most common. Teledyne Optech Inc. (Vaughan, Canada) introduced the Titan multispectral airborne lidar, the first three-wavelength system, equipped with 1550 nm, 1064 nm and 532 nm lasers. The objective of this study was to assess the accuracy of this discrete return multispectral lidar (MSL) for identifying the species of single trees, compared to standard discrete single wavelength lidar. Two distinct datasets were acquired in the Toronto region, Canada. The point clouds of single trees were extracted and 3D and intensity classification features were computed. New intensity features were developed for this purpose, such as lidar NDVIs (normalized difference vegetation index). The species of each tree were identified with a random forest classifier using features calculated from 1) each channel separately and 2) all channels. A stringent selection strategy was employed to reduce the number of features down to 5–9, from 99–142. Trees were classified either as broadleaved (BL) or needleleaf (NL), by genus (4–7 classes), or by species (10 classes). When using all channels, the classification accuracy surpassed what was achieved with single channels, but this advantage was only significant when the number of classes was high, i.e. in the case of seven genera, or ten species. Using MSL data, the out-of-bag error was 3–5% for the BL-NL classification, 13% and 20% for respectively four and seven genera, and 24% for ten species. In the latter case, the best single-channel classification (based on 1550 nm data) resulted in an error of 35%. In the MSL classification, the most useful features were the NDVIs (Normalized Difference Vegetation Index, based on the intensity of infrared and green channels) and the 1550 nm intensities. We therefore conclude that species identification accuracy can be improved by using a three-wavelength ALS such as the Titan system compared to single channel ALS systems, especially when tree species diversity is fairly large (seven classes or more).

1. Introduction

The identification of tree species is critical for forest inventory (Felbermeier et al., 2010), carbon stocks assessment (Jenkins et al., 2003) as well as for habitat and ecosystem change studies (Bradbury et al., 2005; Vastaranta et al., 2014). While the advantages of precise species data for the latter studies are self-evident, it should be underlined that species-specific allometric models for predicting timber volume or above-ground biomass (e.g. as a function of diameter at breast height and height) are more accurate than more general ones (Lambert et al., 2005; Tompalski et al., 2014). For decades, researchers have sought automated remote sensing methods for identifying tree species to replace photo-interpretation, a traditional approach (e.g., in North America and Europe) considered as time-consuming and subjective. Interpreters use three-dimensional appearance (3D), brightness and color cues to recognize species on aerial photography (Leckie et al., 1998; Eid et al., 2004), thus exploiting the architectural and reflectance differences between species. In boreal and temperate forests, important variations in structural characteristics indeed exist between species. The overall crown shape of most spruces (*Picea* sp.) and firs (*Abies* sp.), for example, is pointy and vertically elongated, compared to the roundish crowns of most broadleaved (BL) trees (such as *Acer*, *Betula*, *Populus*). Among needleleaf (NL) trees, branching patterns may differ. For example, white pines (*Pinus strobus*) and Norway spruces (*Picea abies*) seen from above exhibit a star-shaped outline, while white spruces (*Picea glauca*) and American larch (*Larix laricina*) have a smoother and more compact architecture. At least some of these 3D characteristics can be measured using

* Corresponding author.
E-mail address: st-onge.benoit@uqam.ca (B. St-Onge).

http://dx.doi.org/10.1016/j.rse.2017.09.037
Received 4 March 2016; Received in revised form 20 September 2017; Accepted 28 September 2017

airborne laser scanning (ALS) and used to identify species, by computing features, such as the height distribution of laser returns, features extracted using alpha shapes, or 3D textural properties (Vauhkonen et al., 2009; Li et al., 2013). When using single channel ALS (usually 1064 nm or 1550 nm) for basic species identification tasks, such as distinguishing between NL and BL trees or between just two NL species, the achieved accuracies were as high as 95% (Holmgren and Persson, 2004). Separating BL species, or distinguishing between a much larger number of species is however more challenging (Brandtberg, 2007; Kim et al., 2011). Some studies have tried to improve the identification accuracies by using full-waveform ALS features, such as pulse echo width, waveform amplitude, waveform energy, number of echoes, etc. (review: Koenig and Höfle, 2016). Accuracy improvements in species classification by about 6% (Vaughn et al., 2012) or 11% (Yu et al., 2014) were achieved by including full-waveform features, compared to identification based on discrete-return only.

The reflective properties of different species vary according to biochemical attributes of the foliage such as pigment concentration and nitrogen content (Ustin et al., 2009), structural attributes (leaf and stem structures, e.g., LAI and LAD), water content (Asner, 1998) and stem reflectance (Asner et al., 2014). For example, compared to NL species, boreal or temperate BL deciduous trees have leaves with a high growth rate during the short warm season and, consequently, have a large photosynthetic capacity and high concentrations of chlorophyll and nitrogen (Wright et al., 2004). To some degree, these differences can be discriminated based on their spectral signature.

Some limited improvement in tree species identification had been achieved by adding intensity features from the monospectral ALS (Ørka et al., 2009; Korpela et al., 2010b). More recently, a larger number of feature types were derived in a systematic way from 3D and intensity information, with improved results for species classification (Lin and Hyyppä, 2016). In general, approaches for capturing spectral radiometric data in addition to 3D information are comprised of a) using image matching to extract color photogrammetric point clouds from multispectral multi-view airborne images, b) combining single channel ALS to multi- or hyperspectral imagery, or c) combining airborne scanning lasers having different wavelengths. The first approach is still quite recent, but was used for example to identify three different tree boreal species with an accuracy of 89% (St-Onge et al., 2015). The second approach, which proceeds by extracting spectral information at the pixel locations corresponding to ALS first returns, either from multispectral (3–4 spectral bands) imagery (Persson et al., 2004; Holmgren et al., 2008; Ørka et al., 2012), or hyperspectral imagery (Dalponte et al., 2012; review: Ghosh et al., 2014), has brought improvements in the accuracy of species identification. However, coloring ALS points with image intensities requires joining two data sets usually obtained through distinct aerial surveys. Moreover, it is hindered by the complex directional reflectance anisotropy related to the changing sun-object-sensor geometry that influences intensities within and among images (Heikkinen et al., 2011). Considering these limitations, an emerging third approach was developed by using lidar sensors that transmit and receive at several wavelengths (Wang et al., 2013; Hopkinson et al., 2016). In addition to the increased density of the 3D component, the intensity of returns is measured in two or more wavelengths, allowing the creation of spectral signatures potentially useful for species recognition.

ALS intensities depend on the power of the backscattered laser pulses measured by the sensors. Instantaneous received power, explained by the radar equation (Jelalian, 1992; Wagner et al., 2006; Roncat et al., 2014), is determined by acquisition parameters (beam width, aperture, range, etc.) and the effective backscatter cross-section (σ, in m^2) of the reflecting object:

$$\sigma = \frac{4\pi}{\Omega}\rho A \quad (1)$$

where $4\pi/\Omega$ is the scattering angle of the object relative to an isotropic scatterer, ρ its reflectance, and A the object's area within a footprint (silhouette area). A is logically related to leaf area index, and $4\pi/\Omega$ to leaf angle distribution (Asner, 1998), two characteristics that vary between species, but that are wavelength independent. ρ however varies with wavelength and can theoretically enhance species discrimination if multispectral intensity data are acquired. Intensity values are obtained through a process in which the received power at a given time is converted to digital values on an arbitrary scale. In the case of discrete return laser scanners, intensities should be approximately proportional to the power of the received energy at the instant a return is triggered. However, the methods by which intensity values are generated by a given sensor are sometimes proprietary (e.g., for Teledyne Optech sensors) and not disclosed by the ALS system vendors, making it difficult to know exactly how received power is translated to digital values in these cases. It is nevertheless expected that the intensities will be correlated to σ, i.e. at least partly influenced by the values of ρ, which is itself species dependent.

Using ALS multispectral intensities rather than the spectral signature of passive sensors has certain theoretical advantages. The measurements of ALS intensity have the advantage of being independent from external illumination conditions. Because they are all done using the same “hot spot” geometry, the intensity data is not influenced by variable shadowing, leading to lesser variations compared to the aerial imaging case (Woodhouse et al., 2011). In addition, tree and ground signals cannot be separated in passive sensors' measurements of reflectance, whereas the association of the 3D and intensity data in ALS allows this discrimination by imposing a height threshold. Moreover, normalization of the radiometric variations caused by range difference in ALS data can be corrected to some extent for power attenuation due to the travel distance of pulses and their reflection (Korpela et al., 2010a). Several strategies for more advanced radiometric normalization have also been proposed (Yan and Shaker, 2014; review: Kashani et al., 2015).

The first attempts at using multispectral ALS data for land use, or vegetation classification usually had to rely on multiple airborne surveys, each using a single wavelength system. Wang et al. (2013) acquired two wavelength full-waveform ALS data in two separate flights using Optech ALTM Pegasus HD400 (1064 nm) and Riegl LMS-Q680i (1550 nm), and tested their performance in land cover classification. They highlighted the possibility of soil-vegetation separation, and the importance of moisture and physiological information of vegetation for species retrieval. Recently, Hopkinson et al. (2016) compared variation in intensity between discrete ALS point clouds acquired at three different wavelength, each with a different sensor on independent flights (Teledyne Optech's Aquarius - 532 nm, Gemini - 1064 nm, and Orion - 1550 nm). They found that the intensity-based foliage characterization was different for each sensor and was associated with both the sensor's wavelength and the survey sampling characteristics (flight altitude, system settings, etc.). Variations in the latter factors however makes it difficult to combine the intensities of different monospectral ALS to classify land cover or identify tree species using wavelength ratios as NDVI.

The operational advantages of integrating lasers of different wavelengths into a single system led to the development of multispectral laser (MSL) simulations and system prototypes. Some studies were conducted to analyze the variations of NDVI and photochemical reflectance index (PRI) along canopy profiles using a four wavelength airborne MSL (531, 550, 670 or 690, and 780 nm) simulated on virtual forest stands (Morsdorf et al., 2009) or tested in laboratory over living trees (Woodhouse et al., 2011). They demonstrated the possibility of capturing leaf-level physiological variations along vertical profiles and spatially distinguishing the photosynthetic active elements from bark material. Furthermore, different prototypes using a supercontinuum laser source were tested in laboratory. Chen et al. (2010) tested such a MSL prototype for NDVI estimation and collected range and intensity data at 600 nm and 800 nm. In another experiment, a full waveform hyperspectral terrestrial lidar using a supercontinuum laser was developed by Hakala et al. (2012) for the measurement of vegetation features at eight different wavelengths (542, 606, 672, 707, 740, 775, 878, and 981 nm). Nevalainen et al. (2014) used the same hyperspectral terrestrial lidar to test 27 vegetation indices and their relation with the chlorophyll amount. Furthermore Vauhkonen et al. (2013) tested this device for separating pines from spruces using intensity features and NDVI. For leaf nitrogen estimation and for different material classification, Gong et al. (2015) and Wei et al. (2012) tested a MSL with four wavelengths in the visible and infrared spectra (556, 670, 700, and 780 nm) transmitted from four semiconductor laser diodes.

Gaulton et al. (2013) tested the possibility of estimating the vegetation moisture with a full-waveform dual wavelength terrestrial laser scanner system, operating at two wavelengths (1063 and 1545 nm). These studies proved that differences between lidar intensity in different wavelengths could be used to distinguish several characteristics of vegetation which could help in species identification.

The first operational three wavelength airborne laser scanning system was introduced by Teledyne Optech in 2014. The Titan system is comprised of lasers firing at three different angles at the respective wavelengths of 532, 1064 and 1550 nm (see Table 1 for details). The system is fundamentally a discrete return ALS (up to four discrete XYZ returns per pulse), but each channel can be fitted with a waveform digitizer to generate full-waveform data. Compared to combining separate ALS surveys at different single wavelengths, a MSL system has the advantage of mitigating the differences in survey sampling characteristics (flight paths, atmospheric conditions, vegetation phenology, etc.) between the data from the three wavelengths, thus facilitating analysis (Hopkinson et al., 2016). As highlighted by Fernandez-Diaz et al. (2016), three wavelength and three-look angle design provides redundancy and diversity which is beneficial on technical and financial levels. According to the same study, the system can be flown up to 2000 m above ground level.

Fernandez-Diaz et al. (2016) studied the pulse energy characteristics of the laser source as a function of the pulse repetition frequency (PRF). They concluded that the advantage of the Titan fiber laser sources is that the energy per pulse does not degrade significantly as the PRF increases, which used to be the case with the standard monospectral laser systems as Optech's Gemini or Aquarius. Differences in ground return density between channels was attributed to beam divergence, independent laser power between channels and look angles, which resulted in different energy densities at the footprint. Assessment of the range resolution of the Titan system by the same authors showed that its variation between channels is small and insignificantly affected by the PRF, compared to other monospectral systems like Aquarius and Gemini. This improved range resolution could be beneficial for studies about canopy structure.

To date, the majority of studies that tested the Titan system for land cover classification were based on raster images generated using intensity or return height data. For land cover classification, some studies used only intensity data from the three channels (Wichmann et al., 2015; Ahokas et al., 2016; Hopkinson et al., 2016; Morsy et al., 2016), or a combination of 3D and intensity information (Bakuła et al., 2016; Hu, 2016; Matikainen et al., 2016; Zou et al., 2016). In a first study using Titan data to identify a large number of tree species, St-Onge and Budei (2015) used the mean and standard deviation of the intensities extracted from manually delineated crowns. This allowed to identify BL vs. NL trees with a 4.6% error, and distinguish between 8 genera with a 24.3% error. Yu et al. (2017) used Titan data to discriminate between three species (pine, spruce and birch) of which crowns were automatically delineated. They calculated four types of features, respectively based on point cloud, single-channel intensity, multi-channel intensities, and the combined data from the three channels. The best accuracy (85.9%) was obtained using the combined dataset, but was not much higher than that reached using single channels. It appears probable that this limited performance increase could be attributed to the low number of species classes. A higher number of species in a classification model will normally decrease the accuracy of the identification (Baldeck and Asner, 2014), creating a situation where enriched data would be beneficial. We therefore posit that using MSL system datasets in forests having much greater species diversity should lead to a larger accuracy increase compared to single channel ALS results.

Table 1
Titan system's laser characteristics.

Channel	Wavelength	Divergence (1/e)[a]	Forward tilt	Pulse width
C1	1550 nm	0.35 mrad	3.5°	3.0–3.5 ns
C2	1064 nm	0.35 mrad	0.0°	3.0–3.5 ns
C3	532 nm	0.7 mrad	7.0°	2.5–3.0 ns

[a] Paul LaRoque, Teledyne Optech., pers. comm.

The objective of the present study is to evaluate the magnitude of the accuracy gains provided by the three wavelength data of the Titan system compared to single wavelength ALS in the identification of tree species. Three classification levels were considered: species, genus, and BL vs. NL. This represents, to the best of our knowledge, the first attempt to separate a relatively large number of species (10) using an operational MSL system. The general hypothesis is that the combination of ALS data acquired in three wavelengths will markedly enhance the species identification capacity, in this situation characterized by a fairly high diversity of BL and NL species, due to the increased spectral resolution of the data.

2. Data and methods

2.1. Study regions

The MSL datasets used in this study were acquired in two different environments, with a mixture of indigenous and non-indigenous trees: a suburban site with individualized trees along streets, and a partly managed forest comprised of plantations and naturally growing trees. The first MSL dataset was created on October 2, 2014, during a test flight over a 38 ha area located in the district of Scarborough (SC), Ontario, Canada (centered on 79°68′ W, 43°47′ N), a low-density suburb of the city of Toronto. The most common BL genera found in this site are *Acer* and *Fraxinus*, and the most common NL genera are *Picea* and *Pinus*. Sampled trees are situated principally along the streets and are most often isolated so that neighbouring crowns do not interpenetrate. At the time of acquisition, the foliage color of the BL trees had not yet started to change significantly. The topography of this site is essentially flat (Fig. 1).

The second dataset was generated on July 2, 2015, over a 2546 ha site located in the York Regional Forest (YRF), in Ontario, Canada (centered on 79°19′ W, 44°04′ N). This site is characterized by a mix of natural forests (53%) and reforestation/plantation areas (47%), mostly NL trees, which creates a mosaic of various ecosystem types (Regional Municipality of York, 2010). The main species are Norway spruce (*Picea abies*), white spruce (*Picea glauca*), red pine (*Pinus resinosa*), white pine (*Pinus strobus*), Scots pine (*Pinus sylvestris*), American larch (*Larix laricina*), sugar maple (*Acer saccharum*), white ash (*Fraxinus americana*), trembling aspen (*Populus tremuloides*), and red oak (*Quercus rubra*). Most tree stands are dense, with touching or interpenetrating crowns. The characteristics of each survey are summarized in Table 2.

2.2. Multispectral lidar data

Titan MSL discrete return XYZ position and intensity data quantized on a 12 bit scale for the two sites were obtained from Teledyne Optech. The recorded intensity values corresponded to the peak amplitude of each return. The relationship between the received power and the recorded intensities was said to be linear over the entire scale (pers. comm. Paul LaRoque, Teledyne Optech, 28 Oct. 2015).

A quality assessment of the 3D data was performed using various visualization and quantitative strategies by St-Onge and Budei (2015). The inter-channel coregistration, and the inter-swath registration were checked, and no evidence of misregistration was found.

The MSL data have been provided with the range of each return, which allows correction of the intensities for attenuation. The equation of Korpela and Rohrbach (2010) was used for this purpose:

$$I_n = (R/R_{ref})^a I_{raw} \quad (2)$$

where I_n is the range-normalized intensity, I_{raw} is the raw intensity, R the range, and R_{ref} the reference range. The a exponent was set to 2.

2.3. Selection and identification of sample crowns

Sample crowns were selected at both sites for training and evaluating the species classifier. Only the trees having a height of 5 m or more, a minimum crown area of 1 m^2, and having at least one return

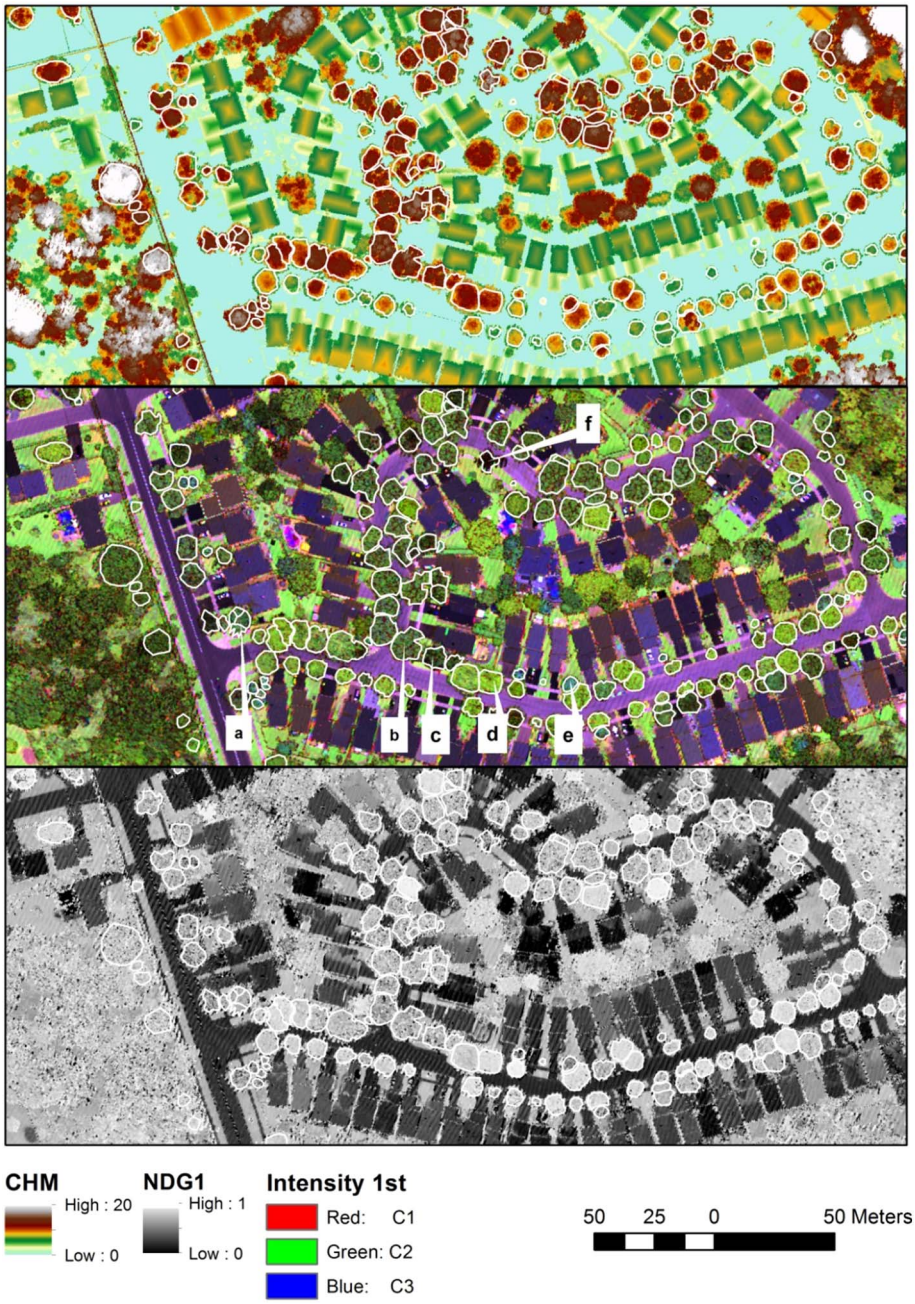

Fig. 1. Canopy height model (top), color composite (red: C1, green: C2, blue: C3) of the three-channel MSL first-return intensities of the SC site with a sample of manually delineated crowns (a = *Pinus*, b = *Fraxinus*, c = *Betula*, d = *Acer*, e = *Picea*; crown f is severely defoliated), and NDVI of type 1 (NDG1, see Table 7). (For interpretation of the references to color in this figure legend, the reader is referred to the web version of this article.)

from each channel were kept. At the SC site, the trees were identified based on a field census of tree species of the Scarborough area (City of Toronto, 2010) and by using Google Street View™. The latter terrestrial images were acquired in the summer of 2014. All trees that were visible from the streets were sampled. At the YRF site, a field survey conducted in August 2015 provided species observations at 400 geolocations. At these locations, observations of single recognizable trees, tree groups of the same species, or dominant species of a given plantation were made. The locations were chosen for their accessibility (along roads or trails) and, where possible, were well spatially distributed (for species found in several locations across the site) to account for potential variations in site conditions and ALS scan angles. Our aim was to select dominant trees stratified in three height classes for each species (5–10 m, 10–20 m, and > 20 m). Because the pre-existing site documentation (stand map, species information, etc.) was fairly general, and many stands were mixed woods, strict stratification of the sample (i.e., *n* trees per height class) was operationally difficult (see Table 3 for height statistics). At this site, aerial photos were acquired at the same time as the MSL data, with the built-in CM-1000 RGB sensor of Teledyne Optech. The images had a ground resolution of approximately 10 cm, which allowed the photo-interpretation of several species with high certainty. These images were used by a photo-interpreter to ensure that the tree crowns delineated on the lidar CHM within groups or plantations were indeed of the species mentioned in the field notes (e.g., so that naturally regenerating BL trees within a pine plantation would not be included). Field observations on defoliated or dead trees were used to train the photo-interpreter to exclude them during the delineation stage, as recognizing trees from different species at various degrees of defoliation was outside the scope of this study. At the YRF site, NL trees were easier to identify by photo-interpretation than BL trees because they were often found in monospecific plantations. Photo-interpretation of BL species being more difficult, their identification came solely from field observations. For this reason, the BL classes had generally fewer individuals than the NL.

Table 2
Survey characteristics.

	SC	YRF
Flight date	2 October 2014	2 July 2015
Pulse repetition frequency/channel (kHz)	200	100
System pulse repetition frequency (kHz)	600	300
Scan frequency (Hz)	52	52
Field of view (degree)	30	30
Mean flight altitude above ground (m)	360	800
Footprint diameter (cm) in C1, C2, C3	12.6, 12.6, 25.2	28, 28, 56
Number of flight lines	3	18
Lateral strip overlap	Approx. 43%	Approx. 50%
Mean number of first returns m^{-2} by channel (C1, C2, C3) of individual flight lines[a]	12.6, 12.8, 12.6	3.4, 3.4, 3.3
Mean number of first returns m^{-2} of all channels (C1, C2, C3) for aggregated flight lines[a]	53.7	20.2

[a] The mean number of first returns m^{-2} were calculated over the entire scanned area, i.e. including all surface types.

Sample trees were identified according to three classification levels: foliage type (BL and NL), genus and species. At the SC site a total of four tree genera were studied (3 BL and 1 NL, see Table 3). For this site, identification was limited to the genus level because there were too few sampled trees per species to have a reasonable minimum number of individuals per class (here established at 30), or because the exact species was sometimes difficult to ascertain due to the possible presence of various cultivars. At YRF site we studied a total of ten species from seven genera (4 BL and 3 NL). The sample contained some relatively isolated trees (crown not touching neighbours), as well as numerous trees growing in closed canopy conditions. Because many of the NL trees were sampled from plantation sites, they came from generally mature and even-aged populations. For red pine, samples were taken from several plantations having different ages. Even if the sample was dominated by mature trees, a relatively better representation of small trees compared to the other NL classes was achieved. The species with uneven-aged populations were mainly broadleaf trees like red oak, or trembling aspen. Height distributions varied between species, the modal height class being for example 20–26 m for Norway spruce, white pine, red pine or sugar maple, but 10–17 m for Scots pine, American larch or white ash (see Table 3).

2.4. Delineation of sample tree crowns

The crowns geolocated in the field or identified in the photo-interpretation were delineated manually using visual interpretation of 2D renderings of the canopy height model, the intensity images (color composite of intensity of the three laser channels) and, in the case of the YRF, the RGB images. Manual delineation was chosen to enable the assessment of species identification accuracy without significant uncertainty caused by automated delineation. Manual delineation however does not guarantee perfect results as, for example, closely growing trees of the same species could appear as being a single crown. This type of error could affect some of the 3D features used for species identification. Figs. 1 and 2 show examples of delineated crowns overlaid on the CHM, multispectral intensity image, and a vegetation index.

2.5. Lidar point cloud statistics of tree crowns

Table 4 presents the density of returns, per channel and overall (C321), within the selected sample crowns and Table 5 gives a general view of the dynamic range of intensities.

2.6. Computation of classification features

To identify tree class at each classification level (foliage type, species and genus), we developed two feature categories: 3D features based on the XYZ data (Table 6) and intensity features (Table 7). The 3D and intensity classification features were computed from MSL returns on a per-crown basis. Returns falling within the delineated polygons were attributed to the corresponding individual tree. Returns lower than 2 m above ground (i.e., above the ground elevation at the crown centroid) were discarded to eliminate signal from the understory or from the ground (i.e., nontree vegetation, exposed soil, road, etc.). Because each of the Titan's laser return is monospectral, the construction of spectral signatures was achieved through object-based binning. i.e. by computing crown-wise statistics. Using the average intensity in each channel theoretically allows the creation of crown spectral signatures. As the cross-section (A) and ρ variations are evened out by averaging crown-wise, the mean effective backscatter cross-section per crown parameter of σ (Eq. (1)) should be obtained. Furthermore, distribution statistics such as standard deviation or intensity percentiles could also reflect species-specific characteristics (Vauhkonen et al., 2013).

A large number of ALS classification features for land use or species identification have been proposed in past studies (see Introduction). In addition, these features are sometimes replicated for different categories of returns (single returns, first of many, all returns, etc.). Multispectral ALS offers the possibility of increasing the number of features, at least by a factor of three in the case of the Titan system. This can however lead to a situation in which an unreasonable number of features complicates analyses (the so-called “curse of dimensionality”). For a given number of training sample, the increase in feature number (dimensions) can lead to a reduction in predicting power (the so-called Hughes effect: Hughes, 1968), and certainly, to difficulties in generalizing the results. For this reason, we have tried to limit the number of features at all stages of the analysis. Overall, the 3D and intensity

Table 3
Number and height (m) statistics of sample crowns.

	NL/BL	Genus	Species	N	Min	Max	Median	Mean	SD
SC	NL	*Picea*		71	7.7	19.2	13.0	12.9	2.6
	BL	*Acer*		184	5.3	23.3	10.3	10.8	3.5
		Fraxinus		71	7.2	23.5	13.8	13.3	3.1
		Gleditsia		36	5.4	19.7	10.6	10.6	3.1
Total				362					
YRF	NL	*Picea*	*abies* (Norway spruce)	204	9.5	30.6	26.3	25.7	3.6
			glauca (White spruce)	223	9.7	26.6	22.0	21.6	2.9
		Pinus	*sylvestris* (Scots pine)	194	6.1	23.3	13.7	14.1	3.2
			resinosa (Red pine)	192	5.6	29.6	23.6	21.8	5.8
			strobus (White pine)	189	9.9	28.8	22.8	22.0	3.6
		Larix	*laricina* (American larch)	186	10.1	29.2	16.7	18.1	4.5
	BL	*Acer*	*saccharum* (Sugar maple)	202	10.2	31.7	23.1	22.2	4.4
		Fraxinus	*americana* (White ash)	45	7.4	23.8	11.8	12.7	3.6
		Populus	*tremuloides* (Trembling aspen)	174	5.2	28.5	19.9	19.3	6.0
		Quercus	*rubra* (Red oak)	49	7.9	26.2	20.1	17.9	5.3
Total				1658					

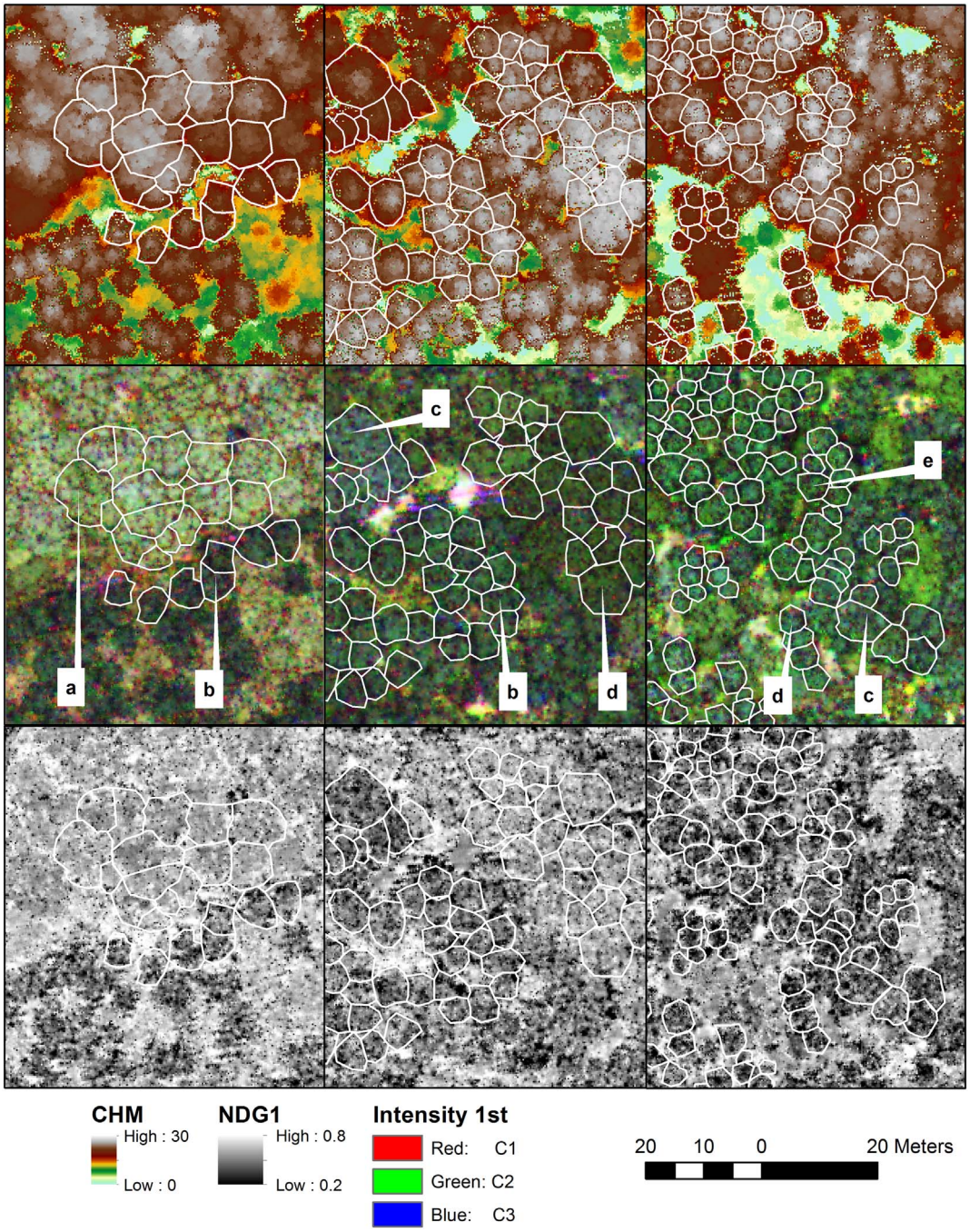

Fig. 2. Canopy height model, color composite (red: C1, green: C2, blue: C3) of the three-channel MSL first-return intensities of the YRF site with a sample of manually delineated crowns (crowns: a = *Acer saccharum*, b = *Pinus resinosa*, c = *Pinus strobus*, d = *Picea glauca*, e = *Picea abies*), and NDVI of type 1 (NDG1, see Table 7). (For interpretation of the references to color in this figure legend, the reader is referred to the web version of this article.)

Table 4
Return density (returns m^{-2}) above 2 m in tree crowns.

	C1	C2	C3	C321
SC				
1st returns	19.8	19.7	19.6	59.1
all returns	29.5	34.8	32.1	96.3
YRF				
1st returns	7.8	7.5	6.1	21.3
all returns	13.4	13.2	8.2	34.8

Table 5
First return intensities above 2 m at different percentiles in tree crowns.

	C1	C2	C3
SC			
5%	22	9	6
50%	218	431	44
95%	376	744	93
YRF			
5%	5	2	3
50%	29	18	9
95%	79	46	20

features are not "complete" with regards to the full set of all features published in the existing literature, and cannot in any case be said to be "exhaustive", as a very wide variety of new features can still be devised. However, we posit that they are sufficient to allow gaining significant knowledge on the new information provided by additional laser channels for the purpose of tree species classification.

Following preliminary tests performed on a wide range of features, we discarded those that did not perform well, were highly redundant, or for which it would be difficult to give a meaningful interpretation. For instance, we restricted the intensity feature computations to the first returns, either the single returns (as these should correspond to hits where the backscatter cross-section profile is highest and transmission losses are high enough to prevent the 2nd echo) or the first of many, depending on the feature (see Table 6). Also, for classification models using intensity features from the three Titan channels, we did not include features computed using the pooled returns from the three channels (which would conflate intra- and inter-channel variances and mix different types of measurements), but kept only those computed separately on each of the three channels. On the contrary, when using the full discrete-return three-channel dataset, the 3D features were computed on the pooled returns from all channels (as the increased density can be advantageous), but not on the separate channels (highly redundant). Depending on the intended goal, 3D features were derived using either the first returns (e.g., for fitting a polynomial on a crown in the case of the SU feature), or all returns (e.g., for the coefficient of variation of return heights). We did not compute features using exclusively single or second returns. A second step in the a priori feature reduction consisted in discarding those that produced spurious or no data values for smaller trees having a low number of returns. When just a few problematic trees occurred, we deleted them instead of discarding the feature. We first present the general principles of the 3D and intensity features. We then explain their nomenclature and provide details on their calculation in Tables 6 and 7. All 3D and intensity features were calculated using the R language (R Core Team, 2015).

2.6.1. 3D features

In the case of 3D features, we wanted to refrain from using absolute measurements, such as tree height or crown area, to ensure that the identification of species would in no case result from a chance association between a given species and specific sizes. For this reason, 3D features were normalized relative to the tree height. This type of normalization was also used for species identification in certain previous studies (Holmgren and Persson, 2004; Ørka et al., 2009). Tree height itself (*H*) was defined as the difference between the elevation of the highest return in the crown and the elevation of the DTM pixel under the crown centroid (read on a 1 m resolution raster DTM). The height of each return within the crown was also computed relatively to this DTM pixel's value, thus avoiding any effect of underlying topography on the 3D shape of crowns (Vega et al., 2014). Different families of 3D features were designed (see Table 6 for details) to capture variations in tree proportions (e.g., AH: ratio of the crown area over the tree height), shape (e.g., SU: curvature of a 3D surface fitted to the crown envelope), slope of the crown profile (SL, or HR: different slope calculations between concentric rings), or porosity (e.g., D1_2: height difference between 1st and 2nd returns of the same pulse, RB: ratios accounting for point distribution in tree height), among other aspects.

2.6.2. Intensity features

Different families of intensity features (see Table 7) were designed to capture the intensity characteristics for the overall crown (mean, dispersion statistics, percentiles), along a vertical gradient (difference between intensity of 1st and 2nd returns), or along a radial gradient (mean intensity by concentric ring). As in the case of 3D features, some ratios between metrics of different return types were computed (RM). Normalized differences between channels were computed to produce NDVI-like features, similar to those used by Wichmann et al. (2015) and Zou et al. (2016).

2.6.3. Feature nomenclature

In Tables 6 and 7, the feature names are presented as a concatenation of type (3D, or intensity - I), followed by the feature family (e.g. SL, NDG1), type of return used, the statistic that was computed, and the channel. For clarification we provide the three following examples of feature names: *3D_SL_all_p50_C321* is a 3D feature that represents the median (p50) of the slope feature family (SL) calculated on all returns of all three channels (C321). *I_NDG1_1st_p75* is an intensity metric that represents the green NDVI of type 1 (NDG1) and is computed using the 75th percentile (p75) of the first returns values in the concerned channels (C3 and C2). *3D_RM_1st_mn_2nd_mn_C3* represents the ratio between the mean height of the first returns (1st_mn) and the mean height of the second returns (2nd_mn) of the third channel (C3).

In the equations found in Tables 6 and 7, the following definitions and symbols are used:

- x, y, z represent the three-dimensional coordinate system;
- i designates each of the n returns within a crown ($i = 1, n$) depending on return type:
  - i_{1st} = first returns,
  - i_{si} = single returns,
  - i_{2nd} = second returns,
  - i_{all} = returns of all types (first, second, etc.), i may also designate any of the possible return types when it appears in a generic equation;
- max is the highest return in a crown;
- d_i represents the horizontal distance between the i^{th} return and the highest return in the crown and calculated as:

$$d_i = \sqrt{(x_i - x_{max})^2 + (y_i - y_{max})^2} \quad (3)$$

- H_{max} is the height of a tree defined as:

$$H_{max} = z_{max} - z_{DTM} \quad (4)$$

where z_{DTM} is the lidar raster DTM height at crown centroid.

H_i corresponds to the height of the i^{th} return within a crown and is given by:

$$H_i = z_i - z_{DTM} \quad (5)$$

- H_{i1} and H_{i2} are the respective heights of the first and second returns of the same pulse.
- I_{i1} and I_{i2} are the respective intensities of the first and second returns of the same pulse.
- R_{max} represents the crown radius defined as the horizontal distance between *max* and the farthest return from it;
- A_j corresponds to each of concentric ring (annulus) of equal width ($R_{max}/4$, with $j = 1,4$) centered on the location of *max*. A_1 is the core circle containing *max*, and A_4 the outside ring.
- m is the slope between *max* and the i^{th} return as given by:

$$m_i = \frac{z_{max} - z_i}{d_i} \quad (6)$$

- V_{chull} represents the volume of the convex hull of the crown computed with the function *chullLiDAR3D* from the R package *rLidar*.

In the "Statistics" column of Tables 6 and 7, *mn* designates the mean, *sd* the standard deviation, *cv* the coefficient of variation (*sd/mn*), *p5*, *p10*, *p25*, *p50*, *p75*, *p90*, *p95* respectively the 5th, 10th, 25th, 50th, 75th, 90th and 95th percentiles, and *lm* is a linear model fit calculated with the *lm* function from the *stats* R package. Moreover, the function *surf.ls* from the R package *spatial* was used to perform a least square fit of a trend surface of the form

$$\widehat{H} = ax^2 + by^2 + cxy + dx + ey + f \quad (7)$$

For conciseness, the "Equation" column in Tables 6 and 7 gives only a few examples of the several possible combinations of return types and feature statistics.

Table 6
Description of 3D features (prefix = 3D_).

Symbol	Description	Return types	Statistics	Equation
AH	Ratio of crown **A**rea over tree **H**eight	–	–	$AH = Crown\ area/H_{max}$
DI	**DI**spersion: coefficient of variation of return heights	all, 1st	cv	$DI\_1st\_cv = cv(H_{i_{1st}})$ $DI\_all\_cv = cv(H_{i_{all}})$
SL	The **SL**ope of the lines connecting the highest return to each other returns	all, 1st	mn, sd, cv, p25, p50, p75	$SL\_mn = \sum_{i=1}^{n-1} m_i/(n-1)$ where (max ≠ *i*); $SL\_p50 = p50(m_i)$; etc.
HR	**H**eight by **R**ings. HR_lm: the slope of a linear model fit (lm) on the H_{A_j} and d_{A_j} values. HR_cv: the coefficient of variation of the H_{A_j} values.	all, 1st	cv	$H_{Aj} = \sum_{i=1}^{nj} H_i/n_j$ where n_j is the number of returns in ring *j*. d_{A_j} is the ring radius at mid-width. $HR\_cv = cv(H_{A_j})$
RB	**R**atio of the number of points in different height **B**ins defined in % of tree height over the total number of points (e.g., 60_80 is the ratio of the number of points in the 60–80% bin over all the points in a crown).	all	Counts: 60_80, 80_90, 90_100, 95_100	$RB_{90\_100} = n_{90-100}/n$ etc.
CH	Ratio of the **C**onvex **H**ull volume over the maximum height cubed.	all	–	$CH = V_{chull}/{H_{max}}^3$
SU	Sum of the two quadratic coefficients (coef) of a least square **SU**rface fit (Eq. (7)) on the H_i values, and average of absolute vertical residual values of the above fit divided by the height of tree (rs).	1st	–	SU_coef = *a* + *b* where *a* and *b* are coefficients of Eq. (7). $rs = \sum_{i=1}^{n} \lvert H_i - \widehat{H_i}\rvert$ $SU\_rs = rs/H_{max}$
D1_2	Height **D**ifference between **1**st and **2**nd return of the same pulse, in the same channel, divided by the height of tree.	–	mn, sd, cv, p25, p50, p75	$\Delta H_{i1\_2} = (H_{i1} - H_{i2})/H_{max}$ $D1\_2\_mn = mn(\Delta H_{i1\_2})$ etc.
RM	**R**atio between different statistics.	all, 1st, 2nd		$RM\_1st\_mn = mn(H_{i_{1st}})/H_{max}$ $RM\_1st\_p50 = p50(H_{i_{1st}})/H_{max}$ $RM\_all\_mn = mn(H_{i_{all}})/H_{max}$ $RM\_all\_p50 = p50(H_{i_{all}})/H_{max}$ $RM\_1st\_p50\_1st\_mn = p50(H_{i_{1st}})/mn(H_{i_{1st}})$ $RM\_1st\_p50\_all\_mn = p50(H_{i_{1st}})/mn(H_{i_{all}})$ $RM\_1st\_mn\_all\_mn = mn(H_{i_{all}})/mn(H_{i_{1st}})$ $RM\_1st\_mn\_2nd\_mn = mn(H_{i_{1st}})/mn(H_{i_{2nd}})$

Table 7
Description of intensity features (prefix = I_).

Symbol	Description	Return types	Statistics	Equations
MI	**M**ean **I**ntensity; Mean intensity of returns between interval of percentiles (5–95, 10–90); Mean intensity between interval of percentile normalized by the overall mean intensity	1st, si	mn	$MI\_mn = mn(I_i)$ $MI\_10\_90\_mn = mn(I_{i_{10,90}})$ $MI\_10\_90\_n\_mn = mn(I_{i_{10,90}})/mn(I_i)$
DI	**DI**spersion: Standard deviation, coefficient of variation	1st, si	sd, cv	$DI\_cv = cv(I_i)$ $DI\_sd = sd(I_i)$
PE	Intensity value at **PE**rcentiles: 5th, 10th, 25th, 50th,75th, 90th, 95th	1st, si	p5, p10, etc.	$PE\_p95 = p95(I_i)$
IR	Standard deviation of the mean **I**ntensity by **R**ing.	1st	sd	The mean return intensity is calculated from returns in each ring $I_{Aj} = \sum_{i=1}^{nj} I_i/n_j$ where n_j is the number of returns in ring *j*. $IR\_sd = sd(I_{A_j})$
D1_2	**D**ifference of intensity between **1**st and **2**nd returns of the same pulse, in the same channel.	–	mn, sd, p25, p50, p75	$\Delta I_{i1\_2} = (I_{i1} - I_{i2})$ $3D\_D1\_2\_mn = mn(\Delta I_{i1\_2})$
RM	**R**atio between different statistics.	all, 1st, 2nd	–	$RM\_1st\_mn\_all\_mn = mn(I_{i_{1st}})/mn(I_{i_{all}})$ $RM\_1st\_mn\_2nd\_mn = mn(I_{i_{1st}})/mn(I_{i_{2nd}})$
NDG1	**G**reen (type **1**) **N**ormalized **D**ifference vegetation index	1st, si	mn, p50, p75	$I\_NDG1\_mn = \frac{mn(I_{iC2}) - mn(I_{iC3})}{mn(I_{iC2}) + mn(I_{iC3})}$
NDG2	**G**reen (type **2**) **N**ormalized **D**ifference vegetation index	1st, si	mn, p50, p75	$I\_NDG2\_mn = \frac{mn(I_{iC1}) - mn(I_{iC3})}{mn(I_{iC1}) + mn(I_{iC3})}$
NDIR	**I**nfra**R**ed **N**ormalized **D**ifference vegetation index	1st, si	mn, p50, p75	$I\_NDIR\_mn = \frac{mn(I_{iC1}) - mn(I_{iC2})}{mn(I_{iC1}) + mn(I_{iC2})}$

2.7. Random forest classification and feature selection

The species class of each tree was identified, at each classification level, using Breiman and Cutler's Random Forests for Classification (RF) approach (Breiman, 2001). This classification method has various advantages, or is sometimes at least equivalent in terms of performance, compared to other methods (Fernández-Delgado et al., 2014). It has been proved to be adequate for species classification in other studies (Korpela et al., 2010b; Ørka et al., 2012). RF does not rely on the assumptions of normality and homoscedasticity. Normality tests (Shapiro-Wilk) on our data revealed that a large proportion of the features did not follow a normal distribution. Also, tests of variance equality between classes (Levene test) indicated that the assumption of homoscedasticity was not fulfilled either. Therefore, some widely used methods such as linear or quadratic discriminant classification could not be directly applied in this case. In addition, RF can handle a very large set of predictors, has a low sensitivity to collinearity between features (Immitzer et al., 2012), and should not overfit (Breiman, 2001). However, RF is sensitive to unbalanced data (large discrepancies in the number of samples per class). Down- or up-sampling strategies to equalize the class frequencies should be applied when the training set itself is unbalanced (Chen et al., 2004).

In accordance with our objectives, we developed classification models using 3D and intensity features *i*) for each of the three Titan channels taken separately (C3, C2, C1), and *ii*) for all channels taken together (C321), including features from two channels in the case of normalized differences. These four options are thereafter referred to as "channel sets". The first group *i*) served to demonstrate the achievable accuracies using single channel ALS, with particular attention to the common 1064 nm and 1550 nm channels. The role of the second group *ii*) was to highlight potential gains brought about by multispectral ALS data.

Despite precautions taken at the design stage, the number of features remained large, varying from 50 to 142. For this reason, we considered different approaches of feature selection. Our goal was to identify a small number of features that jointly provided good species separability using RF classification. Dimensionality reduction strategies through selection or extraction of synthetic features (e.g. principal component analysis) are numerous, and are still the object of active research in the field of pattern recognition where high dimensionality classification problems abound. In ALS-based land-use or species classification, dimensionality reduction was performed for example by testing the classifier using all possible feature combinations (Hovi et al., 2016), an approach that may create a combinatorial burden, or based on the influence of each feature in an initial random forest classification (Yu et al., 2017). Other studies used different algorithms implemented in RF for variable selection and ranking, prior to final species classification (Korpela et al., 2010b; Vauhkonen et al., 2010). We proceeded by first selecting the most useful variables, and then discarded those that were highly inter-correlated. This selection procedure was performed for each site only on the highest available level of classification (genera for SC and species for YRF). A RF trial using all features (Tables 6 and 7) was used to generate an initial accuracy value (mean decrease accuracy) for each feature. The parameter values used in RF were *ntree* = 1501 (RF results do not improve significantly over 300 trees, and odd numbers were preferred to avoid voting ties), *mtry* = 11 (we chose a median *mtry* value to apply for all classification models, after testing the best *mtry* for each level and channel set), and balanced with *sampsize* parameter equal to the minimum number of individuals in a class at a given classification level (36 in the lowest case). The *sampsize* parameter ensures that, at each iteration, the number of sampled crowns was the same in each class. Only features that had a mean decrease accuracy value larger than 0.01 in this initial RF classification were kept. Based on the correlation matrix of the remaining features, we discarded features which had an absolute correlation value larger than 0.9 with another one that had a greater usefulness (larger value of mean decrease accuracy). Consequently, the number of retained features was different for each channel set, depending on the joint usefulness of features and the degree of inter-correlation.

Once the reduced set of features was determined, a RF classification was rerun using only the remaining features. This allowed testing these parsimonious models through the evaluation of their out-of-bag error (for OOB estimate error rate see Liaw and Wiener, 2002; Belgiu and Drăguţ, 2016), with *ntree* = 501, *mtry* = 3 and 100 times randomization for each classification level, and each channel set. For each of these combinations, a confusion matrix was calculated and expressed in percentages, summing up all the resulting confusion matrices of the 100 iterations of RF. The feature selection obtained at the highest classification level for each site was applied at the lower levels. All RF procedures were implemented in the "randomForest" R package (Liaw and Wiener, 2002). Finally, the role of the individual features in class separability was examined through box and whisker plots.

3. Results

The two-step procedure of variable selection using accuracy and inter-correlation criteria produced a number of features much smaller than the initial set (Tables 8 and 9). The number of retained features was equal, or lower, in the case of C321, compared to those of the separate channels. Moreover, even if the initial number of features was greater for SC than for YRF (due to features computed from the difference between 1st and 2nd returns), more features were retained for YRF than for SC. The number of selected features for each combination of site and channel set depended largely on the degree of inter-correlation between features. Those belonging to the same family (e.g. NDG2) were in general strongly inter-correlated as they represented different statistics (e.g. mn, p50, p75) of the same calculated property. The initial number of features in Table 9 was slightly variable because a few features causing no data occurrences for several trees were discarded.

Tables 10 and 11 list the features retained for classification for each region by channel set, by decreasing importance (based on the mean decrease accuracy). For each classification model, selected variables were comprised of intensity and 3D features, except for the C321 of the SC region, which included only intensity features. Features based on normalized differences (NDG) stood out as the most important ones at the two sites for the C321 channel sets. C1 intensity-based features were the single channel features most useful in the C321 feature sets. At YRF, only two out of nine selected features were based on 3D data. They also had low ranks (7^{th} and 8^{th}). For the two sites, the proportion of 3D features was higher in the single channel sets compared to the C321 channel sets. In all cases the first feature was always an intensity feature. The 3D features were more represented at YRF than at SC, and were the more frequent type for channels considered separately.

Figs. 3 and 4 illustrate the class separability at the highest classification level for each selected feature of C321 at both sites. No two classes were perfectly separated using any given single feature, but some stood out as having only a small overlap with the rest, such as the *Picea* genus at SC using NDG1 and NDG2 features, or sugar maple at YRF with I_PE_1st_p75_C1. Other features that contributed most to the separability of some classes should also be highlighted. The normalized green vegetation indices (NDG) generally had higher value for BL species than for NL ones, as in the case of optical imagery. Ash was

Table 8
Number of features retained at each step of selection (SC).

Elimination step	C3 (532 nm)	C2 (1064 nm)	C1 (1550 nm)	C321
Initial	68	68	68	142
Accuracy filter	16	20	18	19
Correlation filter	7	5	5	5

Table 9
Number of features retained at each step of selection (YRF).

Elimination step	C3 (532 nm)	C2 (1064 nm)	C1 (1550 nm)	C321
Initial	51	49	51	99
Accuracy filter	23	22	23	33
Correlation filter	11	11	14	9

however confounded with NL species at YRF, based on NDG values. The infrared-based index (NDIR) provided less separability power, but was useful for example in separating white pines from other BL species. The two 3D features at species level brought limited discriminative power, but helped for example in isolating Norway spruce from the rest of the BL species. Overall, it is clear that combining all features results in a good level of separability. For example, while Scots pines and white pines are confused with NDG-based features, but distinct from red pines, white pines can be partly isolated from the two other pine species using other features, such as I_PE_1st_p75_C1.

Tables 12 and 13 show the species identification OOB errors of random forest classifications for the different channel sets and sites. The values reported in these tables represent the means of the different OOB values obtained for a given model through 100 random iterations. The standard deviation of these OOB error values never exceeded 0.55% per classification model. The best results at all levels of classification were obtained using the pooled data from the three channels (C321). Interestingly, this was achieved using a number of features lower or equal to that of the single channels. The contrast between C321 results on the one hand, and single channel results on the other hand, became greater as the number of classes increased. The difference between the best single channel classification model (most often C1) and the corresponding C321 model became appreciable only when classifying into seven genera, or 10 species at the YRF site. Except for the BL vs. NL classification level at SC, C3 results were the least accurate.

Confusion matrices for the C321-based species identification presented in Tables 14 to 17 are calculated as a weighted mean error of the 100 random iterations. Confusion matrices presenting absolute counts for a single iteration are given in the Appendix (Tables A1 to A4). At the most general classification level (Table 14), omission and commission errors behave somewhat differently between the two study regions, but the errors are so low that this may be simply anecdotal. At the genus level, the accuracies do not vary sharply between classes, with intervals of 78.9% to 91.6% for SC, and 63.3% to 90.6% at YRF. No marked performance differences were seen between the BL and NL genera accuracies. At both sites, maples had the highest accuracy among BL trees, while oaks at the YRF site had the highest error.

The confusion matrix at species level (Table 17) contains results that could be expected based on the more general classification levels, i.e. higher confusion rates occur among NL species, or among BL species, but rarely between a NL and a BL species. Notable exceptions were the higher levels of confusion between poplars and red pines, and between red oaks and white pines. The highest rate of confusion is the commission error of 20.4% of red oaks towards sugar maples, while the overall highest accuracy was achieved for sugar maple.

4. Discussion

4.1. Feature selection

For reducing the large number of initial 3D and intensity features, especially in the multispectral case, we selected the most useful and less redundant ones based on thresholds of mean decrease accuracy and inter-correlation between features. The final selection of features varied between study sites, and classification levels. We consider futile to discuss minute details of the feature selection results, such as the fact that the 75th intensity percentile was the first variable in the C1 channel set while the 90th came out first for C2 (species level at YRF, see Table 11). However, general trends are quite informative on the usefulness of the broad categories of variables. Firstly, for all channel sets and sites, intensity-based features ranked first, and in the case of the C321 set, normalized differences were the most useful. This behaviour was also observed by Yu et al. (2017) in a study using Titan ALS data for identifying two NL and one BL species where an intensity feature and a normalized difference feature were respectively the first and second most important variables in the three-channel set, and a channel ratio was first among the combined intensity variables. In our study, seven out of the nine most useful related features were intensity-based, while four out of the five best features in Yu et al. (2017) were also computed from intensity. These trends indicate that, regardless of the relationship between species and architectural traits of trees, and despite tripling the density of the 3D data in the case of the C321 channel set, variations in monospectral, but especially multispectral intensities, carry more information on species than 3D data. In searching for explanations for these findings, it should be remembered that the intensity values depend not only on the reflectance of the foliage, but also on its orientation and on the area of its cross-section within each laser footprint. Differences in this regard between NL and BL species are expected to be large. This fact was confirmed, among other observations, by sugar maples having the highest intensities in all but one of the single intensity plots of Figs. 3 and 4. Sugar maples have large and overlapping leaves, a planophile leaf angle distribution, and a high infrared reflectance, thus generating powerful returns. They had the largest ratio of number of single returns over number of first returns (not presented). NDVI-like features were very useful for species identification probably because they capture, in the case of NDG1 and NDG2, the variations between the green (linked to the chlorophyll contents) and the infrared (related to the foliar structure and water content) parts of the spectrum. C1-based features (1550 nm) were also quite frequent among the most useful variables, showing the utility of this wavelength. C3-based single-channel features seldom appeared (but C3 was present in most normalized differences). The wider divergence and longer ranges due to the 7° firing angle in C3 resulted in a lower incidence power at leaf level, and thus, the laser irradiance at canopy level in this channel should be lower than in the infrared channels. In addition, the reflectance of foliage at 532 nm is much lower than in the infrared. For these reasons, it is expected that the signal to noise ratio in C3 should be much smaller than in the other channels. Nevertheless, a C3 intensity-based feature ranked first, i.e. above 3D features, in both regions when classification was carried out using the C3 channel set.

Table 10
Selected features (SC).

C3 (532 nm)	C2 (1064 nm)	C1 (1550 nm)	C321
I_RM_1st_mn_all_mn_C3	I_PE_1st_p95_C2	I_PE_1st_p95_C1	I_NDG2_si_mn
I_CT_si_mn_C3	3D_PE_1st_p50_C2	I_D1_2_sd_C1	I_PE_1st_p95_C1
I_D1_2_p75_C3	I_DI_si_sd_C2	3D_SL_1st_p50_C1	I_PE_si_p75_C2
I_D1_2_mean_C3	I_D1_2_sd_C2	3D_SL_all_p25_C1	I_D1_2_sd_C1
3D_RM_1st_mn_all_mn_C3	I_RM_1st_mn_all_mn_C2	3D_SL_all_p50_C1	I_NDG1_si_mn
3D_SL_all_p75_C3			
3D_SL_1st_mn_C3			

Table 11
Selected features (YRF).

C3 (532 nm)	C2 (1064 nm)	C1 (1550 nm)	C321
I_PE_si_p75_C3	I_PE_1st_p90_C2	I_PE_1st_p75_C1	I_NDG1_1st_p75
3D_CH_all_C3	3D_SL_all_p75_C2	I_DI_1st_sd_C1	I_NDG2_1st_mn
3D_PE_all_p25_C3	3D_CH_all_C3	3D_CH_all_C1	I_DI_1st_sd_C2
3D_PE_all_p50_C3	3D_RM_1st_mn_all_mn_C2	3D_SL_1st_p75_C1	I_NDIR_1st_p75
I_DI_si_sd_C3	3D_SL_all_p25_C2	3D_RM_1st_mn_all_mn_C1	I_PE_1st_p75_C1
I_IR_1st_C3	3D_SL_all_p50_C2	3D_HR_all_lm_C1	I_PE_si_p75_C3
I_DI_1st_cv_C3	3D_SL_1st_p50_C2	I_RB_05_95_1st_C1	3D_RM_1st_mn_2nd_mn_C321
3D_MI_all_mn_C3	3D _RM_1st_mn_2nd_mn _C2	3D_RM_1st_mn_2nd_mn_C1	3D_SL_all_mn_C321
I_PE_1st_p50_C3	3D_HR_all_lm_C2	3D_SL_all_mn_C1	I_DI_1st_sd_C1
3D_PE_all_p75_C3	I_RM_1st_mn_all_mn_C2	3D_SL_all_p50_C1	
I_PE_1st_p25_C3	3D_RM_all_p50_all_mn_C2	3D_SL_all_p25_C1	
		3D_SL_1st_mn_C1	
		3D_RM_all_mn_C1	
		I_PE_1st_p25_C1	

4.2. Accuracy improvements in species identification

The results presented above demonstrate that the additional information provided by the two extra wavelengths of the Titan MSL, compared to single channel ALS sensors, improved species classification at all classification levels and sites, with an effect strongly proportional to the number of classes. Because there have been very few studies on species identification with three wavelength ALS, we are quite limited when trying to compare our results to those of other researchers. Even in the case of single-wavelength ALS species identification studies, comparing the respective accuracies reported in previous studies is quite arduous because the number of species, the size of trees, and different acquisition parameters vary between them. Such research efforts were so far presented by Hopkinson et al. (2016) and Yu et al. (2017). The former researchers were able to separate tree classes (broadleaf, larch and pine/spruce trees at plot level, Titan data acquired at a height of 800 m above ground level) with an accuracy between 66% and 80%, but did not compare to single channel results. Yu et al. (2017) obtained an accuracy of 86% when combining features from all three channels for identifying three species (pine, spruce and birch at individual tree level, data acquired at 400 m above sea level), which was not significantly different from the best performance using single channel. In our study, the advantages of three-channel ALS became significant for classifications with seven or more classes. Even in the case of the identification of four genera, gains relative to single-wavelength ALS were marginal, a result that is compatible to those of Yu et al. (2017). Evidently, having a greater number of species brings more variability in the shape, size and reflectance of leaves, and in tree architecture, creating a more difficult identification task. In this case, the added information contents of the Titan data allowed us to identify as many as 10 species with an accuracy superior to 75% using as little as nine features from MSL only. To the best of our knowledge, such results had not yet been reported in the scientific literature.

4.3. Limitations and generalizability

The error levels reported in this paper apply to manually delineated crowns. It is probable that these levels would rise in the case of automatically delineated crowns due to unavoidable random or systematic segmentation errors. Moreover, it can be expected that species identification of smaller trees is more difficult than that of larger ones, simply because the number of returns (at a given point density) will then be lower. The 3D characteristics would then be less well defined and the per-crown intensity statistics noisier. The majority of classification studies limit their research to trees having commercially valuable sizes. Having a diversity of tree ages in the sampled crowns comparatively increase the intra-species variability and the classification error probability because of the changes in tree architecture, leaf shapes and reflectance with tree age. Further research must be done to understand if stratification by tree height or age could improve classification performance, as remarked also by Hovi et al. (2016). Furthermore, the random forest model trained with a limited sample coming from a specific region is difficult to apply on a broader scale without additional training samples to account for site variation.

Both datasets used in the present study covered rather small areas and were each surveyed over a short period of time during which no significant changes occurred in the atmospheric or surface conditions that could have affected pulse attenuation. Furthermore, the sampling density (crown samples/km^2) was relatively high, creating very good conditions for training a classifier, at the cost however of numerous hours of field work and

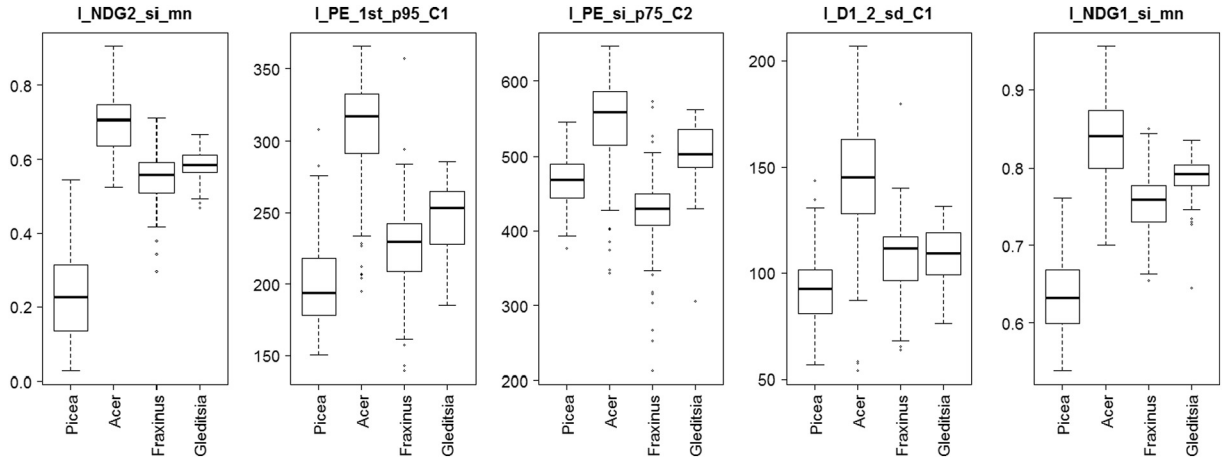

Fig. 3. Variation of selected variables at genus level (SC).

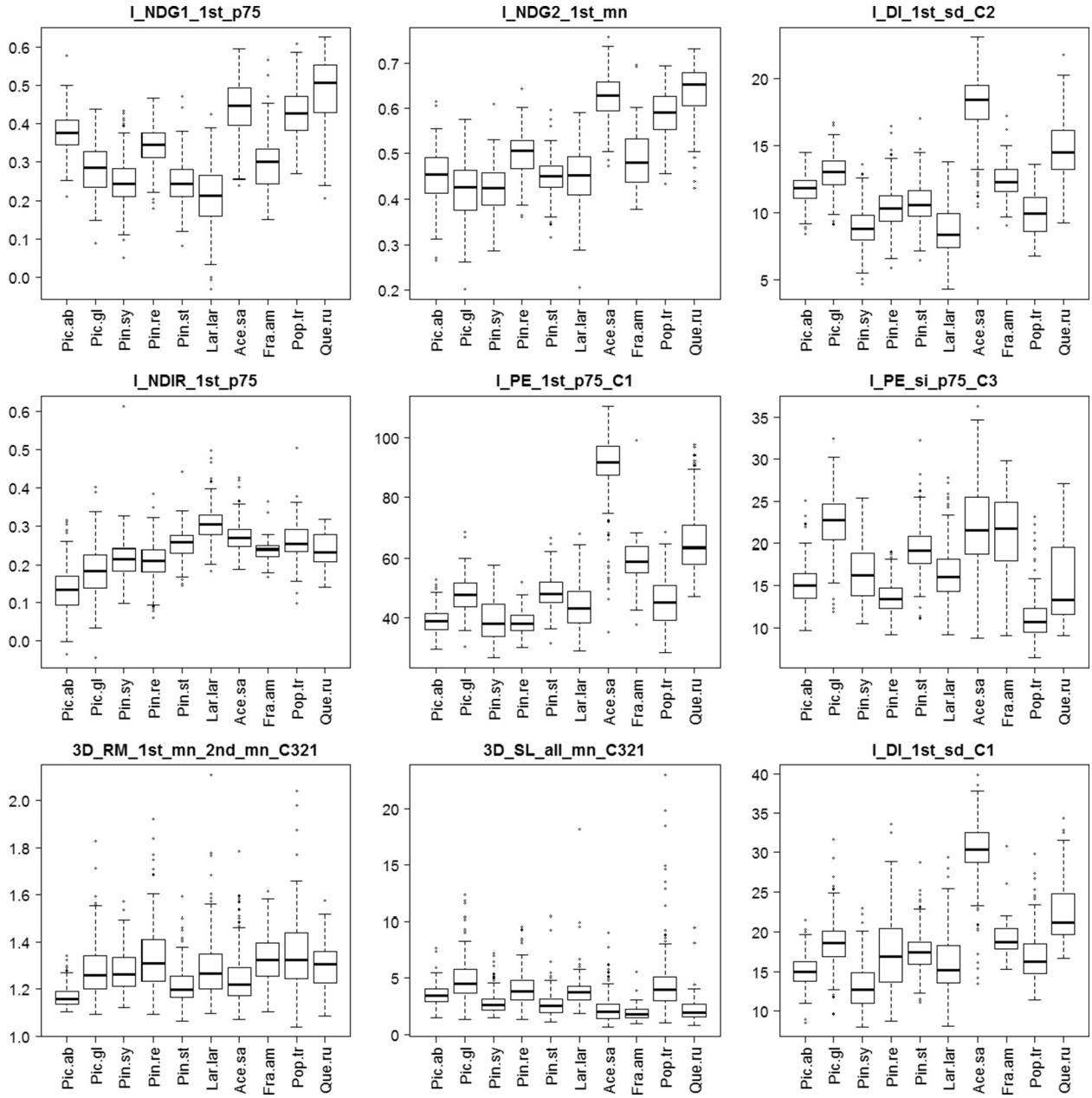

Fig. 4. Variation of selected variables at species level (YRF).

Table 12
Identification OOB error rate (SC).

Laser channels	C3 (532 nm)	C2 (1064 nm)	C1 (1550 nm)	C321
Number of features	8	6	6	6
BL vs. NL	3.0%	6.6%	5.3%	2.8%
4 genera	24.6%	21.8%	15.8%	13.3%

Table 13
Identification OOB error rate (YRF).

Laser channels	C3 (532 nm)	C2 (1064 nm)	C1 (1550 nm)	C321
Number of features	11	11	14	9
BL vs. NL	14.2%	12.3%	10.2%	4.6%
7 genera	36.7%	29.9%	31.3%	19.9%
10 species	38.4%	35.9%	34.7%	23.6%

Table 14
Confusion matrix in % for C321 at BL/NL level.

	SC		YRF	
	NL	BL	NL	BL
NL	**94.4**	5.6	**96.4**	3.6
BL	2.1	**97.9**	7.2	**92.8**

Numbers in bold represent the percentage of correctly identified tree species.

interpretation. Deploying this approach over larger territories, using surveys carried out on different days, i.e. encompassing varying surface and atmospheric conditions, could certainly lead to complications. While it can be assumed that basic 3D features, such as tree proportions or overall shape for a given species at a given age, would be relatively stable over a larger region, intensities might be affected by variations in foliage humidity (especially in the 1550 nm channel), or in atmospheric transmissivity between survey days.

Table 15
Confusion matrix in % at genus level (SC).

	Picea	*Acer*	*Fraxinus*	*Gleditsia*
Picea	**91.6**	1.4	7.0	0.0
Acer	0.0	**88.0**	7.1	4.9
Fraxinus	7.0	5.6	**78.9**	8.5
Gleditsia	0.0	0.0	13.9	**86.1**

Numbers in bold represent the percentage of correctly identified tree species.

Table 16
Confusion matrix in % at genus level (YRF).

	Picea	*Pinus*	*Larix*	*Acer*	*Fraxinus*	*Populus*	*Quercus*
Picea	**85.7**	7.7	4.2	0.5	0.5	1.2	0.2
Pinus	7.8	**73.4**	9.9	0.2	4.3	3.7	0.7
Larix	1.1	9.7	**81.7**	0.0	2.7	4.8	0.0
Acer	0.0	0.5	0.5	**90.6**	1.5	2.5	4.5
Fraxinus	4.4	6.7	2.2	2.2	**68.9**	11.1	4.4
Populus	1.1	8.0	2.3	0.0	2.9	**82.2**	3.4
Quercus	0.0	6.1	0.0	20.4	4.1	6.1	**63.3**

Numbers in bold represent the percentage of correctly identified tree species.

Table 17
Confusion matrix in % at species level (YRF).

	Pic.ab	*Pic.gl*	*Pin.sy*	*Pin.re*	*Pin.st*	*Lar.lar*	*Acer.sa*	*Fra.am*	*Pop.tr*	*Que.ru*
Pic.ab	**83.8**	2.9	1.5	7.8	1.5	1.0	0.0	0.0	1.5	0.0
Pic.gl	0.9	**86.1**	1.8	0.9	6.3	3.1	0.4	0.0	0.4	0.0
Pin.sy	0.5	4.1	**63.4**	10.8	11.3	5.2	0.0	3.6	1.0	0.0
Pin.re	6.3	0.0	13.5	**72.9**	0.5	3.6	0.0	0.0	3.1	0.0
Pin.st	3.2	7.9	6.3	2.1	**64.6**	10.1	0.0	3.7	1.1	1.1
Lar.lar	0.5	3.2	8.1	0.5	7.5	**73.1**	0.0	2.7	4.3	0.0
Acer.sa	0.0	0.0	0.0	0.0	0.5	0.5	**90.6**	1.5	2.5	4.5
Fra.am	0.0	4.4	0.0	0.0	8.9	2.2	2.2	**66.7**	11.1	4.4
Pop.tr	0.0	1.1	0.0	8.0	1.7	1.7	0.0	2.9	**81.0**	3.4
Que.ru	0.0	0.0	0.0	0.0	8.2	0.0	20.4	6.1	8.2	**57.1**

Pic.ab = *Picea abies*, Pic.gl = *Picea glauca*, Pin.sy = *Pinus sylvestris*, Pin.st = *Pinus strobus*, Lar.lar = *Larix laricina*, Fra.am = *Fraxinus Americana*, Pop.tr = Populous tremuloides, Que.ru = *Quercus rubra*.
Numbers in bold represent the percentage of correctly identified tree species.

While the latter can be corrected to some extent (Yan and Shaker, 2014), the effects of foliage humidity variations might be difficult to model. This in turn could create the obligation of gathering costly training data for each flight. On a broader level, variations for example in tree architecture with age or site characteristics (Hovi et al., 2016), or changes in foliage reflectance caused by leaf maturation during the leaf-on season (Kim, 2010; Hakala et al., 2015) or by stress (Gaulton et al., 2013; Gong et al., 2015), would affect the results of any ALS-based species identification, whether in the single or multi-channel case. Further methodological or technological developments are required before a truly robust approach can come about. Nevertheless, our study, by comparing the respective species identification accuracy of single-channel and three-channel lidar data has clearly demonstrated the advantages of using multispectral ALS data for a single tree crown classification. This will hopefully provide better forest data for informing management decisions, as well as a clearer picture of the complex mosaic of species of mixed forest ecosystems.

5. Conclusion

The additional laser channels in airborne MSL, compared to single channel ALS, were shown to be useful for increasing the accuracy in species identification. A significant increase was achieved only when the number of species classes was relatively high. Discrimination between broadleafs and needleleaf species (two classes) did not significantly benefit from MSL data. The additional intensities, and especially channel ratios like NDVIs, were the features that improved most the classification accuracy. 3D features performed well for a limited number of species and for single channels, but their discrimination power was surpassed by intensity features.

Considering the usefulness of MSL intensities, future efforts are needed to improve lidar intensity standardization within large areas. Finally, the features' sensitivity to the intra-species variability caused by tree age, height and growth conditions will need to be further researched.

Acknowledgements

We express gratitude to Teledyne Optech Incorporated (Vaughan, Canada) for graciously providing the Titan MSL datasets used in this study. We also thank the authorities of the York Regional Forest (namely Kevin Reese) for granting permission and facilitating access to the YRF study area. We acknowledge the collaboration of CarboMap (Edinburgh, Scotland) in field logistics and data collection. This study was partly funded by the National Science and Engineering Council of Canada, through the AWARE project (NSERC File: CRDPJ 462973 – 14, Grantee: N.C. Coops, FRM, UBC). We acknowledge the reviewers for the useful comments which help us improve our work.

Appendix A

Table A1
Confusion matrix for C321 at BL/NL level.

	SC			YRF		
	NL	BL	Class error	NL	BL	Class error
NL	**69**	2	0.03	**1161**	27	0.02
BL	5	**286**	0.02	29	**441**	0.06

Numbers in bold represent the percentage of correctly identified tree species.

Table A2
Confusion matrix at genus level (SC).

	Picea	*Acer*	*Fraxinus*	*Gleditsia*	Class error
Picea	**71**	0	0	0	0.00
Acer	1	**164**	13	6	0.11
Fraxinus	5	5	**57**	4	0.20
Gleditsia	1	2	5	**28**	0.22

Numbers in bold represent the percentage of correctly identified tree species.

Table A3
Confusion matrix at genus level (YRF).

	Picea	*Pinus*	*Larix*	*Acer*	*Fraxinus*	*Populus*	*Quercus*	Class error
Picea	**388**	16	12	0	3	8	0	0.09
Pinus	43	**468**	32	1	14	17	0	0.19
Larix	3	11	**167**	0	1	3	1	0.10
Acer	1	5	2	**182**	1	4	7	0.10
Fraxinus	1	1	0	2	**34**	4	3	0.24
Populus	2	7	3	0	7	**149**	6	0.14
Quercus	0	2	1	12	2	3	**29**	0.41

Numbers in bold represent the percentage of correctly identified tree species.

Table A4
Confusion matrix at species level (YRF).

	Pic.ab	*Pic.gl*	*Pin.sy*	*Pin.re*	*Pin.st*	*Lar.lar*	*Acer.sa*	*Fra.am*	*Pop.tr*	*Que.ru*	Class error
Pic.ab	**177**	8	4	3	7	1	0	0	4	0	0.13
Pic.gl	5	**202**	1	2	8	1	0	2	2	0	0.09
Pin.sy	3	6	**139**	13	15	9	1	5	3	0	0.28
Pin.re	11	2	27	**143**	3	2	0	2	2	0	0.26
Pin.st	5	13	16	6	**133**	9	0	3	4	0	0.30
Lar.lar	1	8	3	3	13	**155**	0	0	3	0	0.17
Acer.sa	0	2	2	3	1	0	**181**	1	4	8	0.10
Fra.am	0	1	0	1	1	0	2	**34**	2	4	0.24
Pop.tr	1	1	3	4	2	3	0	4	**149**	7	0.14
Que.ru	0	0	1	0	1	0	12	2	3	**30**	0.39

Pic.ab = *Picea abies*, Pic.gl = *Picea glauca*, Pin.sy = *Pinus sylvestris*, Pin.st = *Pinus strobus*, Lar.lar = *Larix laricina*, Fra.am = *Fraxinus Americana*, Pop.tr = Populous tremuloides, Que.ru = *Quercus rubra*.
Numbers in bold represent the percentage of correctly identified tree species.

References

Ahokas, E., Hyyppä, J., Yu, X., Liang, X., Matikainen, L., Karila, K., Litkey, P., Kukko, A., Jaakkola, A., Kaartinen, H., Holopainen, M., Vastaranta, M., 2016. Towards automatic single-sensor mapping by multispectral airborne laser scanning. In: Halounova, L., Bredif, M., Pajdla, T., Oude Elberink, S., Safar, V., Skaloud, J., Rottensteiner, F., Stilla, U., Limpouch, A., Schindler, K., Mayer, H., Mallet, C. (Eds.), 23rd International Archives of the Photogrammetry, Remote Sensing and Spatial Information Sciences Congress, ISPRS 2016. International Society for Photogrammetry and Remote Sensing, pp. 155–162.

Asner, G.P., 1998. Biophysical and biochemical sources of variability in canopy reflectance. Remote Sens. Environ. 64, 234–253.

Asner, G.P., Martin, R.E., Carranza-Jiménez, L., Sinca, F., Tupayachi, R., Anderson, C.B., Martinez, P., 2014. Functional and biological diversity of foliar spectra in tree canopies throughout the Andes to Amazon region. New Phytol. 204, 127–139.

Bakuła, K., Kupidura, P., Jełowicki, Ł., 2016. Testing of land cover classification from multispectral airborne laser scanning data. Int. Arch. Photogramm. Remote. Sens. Spat. Inf. Sci. XLI-B7, 161–169.

Baldeck, C.A., Asner, G.P., 2014. Improving remote species identification through efficient training data collection. Remote Sens. 6, 2682–2698.

Belgiu, M., Drăguţ, L., 2016. Random forest in remote sensing: a review of applications and future directions. ISPRS J. Photogramm. Remote Sens. 114, 24–31.

Bradbury, R.B., Hill, R.A., Mason, D.C., Hinsley, S.A., Wilson, J.D., Balzter, H., Anderson, G.Q.A., Whittingham, M.J., Davenport, I.J., Bellamy, P.E., 2005. Modelling relationships between birds and vegetation structure using airborne LiDAR data: a review with case studies from agricultural and woodland environments. Ibis 147, 443–452.

Brandtberg, T., 2007. Classifying individual tree species under leaf-off and leaf-on conditions using airborne lidar. ISPRS J. Photogramm. Remote Sens. 61, 325–340.

Breiman, L., 2001. Random forests. Mach. Learn. 45, 5–32.

Chen, C., Liaw, A., Breiman, L., 2004. Using random forest to learn imbalanced data. In: Department of Statistics, University of California, Berkeley. http://www.stat.berkeley.edu/tech-reports/666.pdf, Accessed date: 15 September 2017.

Chen, Y., Räikkönen, E., Kaasalainen, S., Suomalainen, J., Hakala, T., Hyyppä, J., Chen, R., 2010. Two-channel hyperspectral LiDAR with a supercontinuum laser source. Sensors 10, 7057.

City of Toronto, 2010. Every tree counts. A portrait of Toronto's Urban Forest. https://www.itreetools.org/resources/reports/Toronto_Every_Tree_Counts.pdf, Accessed date: 15 September 2017.

Dalponte, M., Bruzzone, L., Gianelle, D., 2012. Tree species classification in the Southern Alps based on the fusion of very high geometrical resolution multispectral/hyperspectral images and LiDAR data. Remote Sens. Environ. 123, 258–270.

Eid, T., Gobakken, T., Næsset, E., 2004. Comparing stand inventories for large areas based on photo-interpretation and laser scanning by means of cost-plus-loss analyses. Scand. J. For. Res. 19, 512–523.

Felbermeier, B., Hahn, A., Schneider, T., 2010. Study on user requirements for remote sensing applications in forestry. In: Szekely, B., Wagner, W. (Eds.), ISPRS Technical Commission VII Symposium on Advancing Remote Sensing Science. International Society for Photogrammetry and Remote Sensing, pp. 210–212.

Fernández-Delgado, M., Cernadas, E., Barro, S., Amorim, D., 2014. Do we need hundreds of classifiers to solve real world classification problems? J. Mach. Learn. Res. 15, 3133–3181.
Fernandez-Diaz, J.C., Carter, W.E., Glennie, C., Shrestha, R.L., Pan, Z., Ekhtari, N., Singhania, A., Hauser, D., Sartori, M., 2016. Capability assessment and performance metrics for the titan multispectral mapping Lidar. Remote Sens. 8, 936.
Gaulton, R., Danson, F.M., Ramirez, F.A., Gunawan, O., 2013. The potential of dual-wavelength laser scanning for estimating vegetation moisture content. Remote Sens. Environ. 132, 32–39.
Ghosh, A., Fassnacht, F.E., Joshi, P.K., Koch, B., 2014. A framework for mapping tree species combining hyperspectral and LiDAR data: role of selected classifiers and sensor across three spatial scales. Int. J. Appl. Earth Obs. Geoinf. 26, 49–63.
Gong, W., Sun, J., Shi, S., Yang, J., Du, L., Zhu, B., Song, S., 2015. Investigating the potential of using the spatial and spectral information of multispectral LiDAR for object classification. Sensors 15, 21989–22002.
Hakala, T., Suomalainen, J., Kaasalainen, S., Chen, Y., 2012. Full waveform hyperspectral LiDAR for terrestrial laser scanning. Opt. Express 20, 7119–7127.
Hakala, T., Nevalainen, O., Kaasalainen, S., Mäkipää, R., 2015. Technical Note: Multispectral lidar time series of pine canopy chlorophyll content. Biogeosciences 12, 1629–1634.
Heikkinen, V., Korpela, I., Tokola, T., Honkavaara, E., Parkkinen, J., 2011. An SVM classification of tree species radiometric signatures based on the Leica ADS40 sensor. IEEE Trans. Geosci. Remote Sens. 49, 4539–4551.
Holmgren, J., Persson, Å., 2004. Identifying species of individual trees using airborne laser scanner. Remote Sens. Environ. 90, 415–423.
Holmgren, J., Persson, Å., Söderman, U., 2008. Species identification of individual trees by combining high resolution LiDAR data with multi-spectral images. Int. J. Remote Sens. 29, 1537–1552.
Hopkinson, C., Chasmer, L., Gynan, C., Mahoney, C., Sitar, M., 2016. Multisensor and multispectral LiDAR characterization and classification of a forest environment. Can. J. Remote. Sens. 42, 501–520.
Hovi, A., Korhonen, L., Vauhkonen, J., Korpela, I., 2016. LiDAR waveform features for tree species classification and their sensitivity to tree- and acquisition related parameters. Remote Sens. Environ. 173, 224–237.
Hu, B., 2016. Improving individual tree delineation using multiple-wavelength lidar data. In: International Geoscience and Remote Sensing Symposium (IGARSS), pp. 3182–3185.
Hughes, G., 1968. On the mean accuracy of statistical pattern recognizers. IEEE Trans. Inf. Theory 14, 55–63.
Immitzer, M., Atzberger, C., Koukal, T., 2012. Tree species classification with Random forest using very high spatial resolution 8-band worldView-2 satellite data. Remote Sens. 4, 2661–2693.
Jelalian, A.V., 1992. Laser radar systems. Artech House, Boston.
Jenkins, J.C., Chojnacky, D.C., Heath, L.S., Birdsey, R.A., 2003. National-scale biomass estimators for United States tree species. For. Sci. 49, 12–35.
Kashani, A.G., Olsen, M.J., Parrish, C.E., Wilson, N., 2015. A review of LIDAR radiometric processing: From ad hoc intensity correction to rigorous radiometric calibration. Sensors 15, 28099–28128.
Kim, S., 2010. LIDAR-based species classification using multivariate cluster analysis. In: American Society for Photogrammetry and Remote Sensing Annual Conference 2010: Opportunities for Emerging Geospatial Technologies. Curran Associates, Inc., San Diego, CA, pp. 405–416.
Kim, S., Hinckley, T., Briggs, D., 2011. Classifying individual tree genera using stepwise cluster analysis based on height and intensity metrics derived from airborne laser scanner data. Remote Sens. Environ. 115, 3329–3342.
Koenig, K., Höfle, B., 2016. Full-waveform airborne laser scanning in vegetation studies-a review of point cloud and waveform features for tree species classification. Forests 7.
Korpela, I., Rohrbach, F., 2010. Variation and anisotropy of reflectance of forest trees in radiometrically calibrated airborne line sensor images - implications to species classification. In: Szekely, B., Wagner, W. (Eds.), ISPRS Technical Commission VII Symposium on Advancing Remote Sensing Science. International Society for Photogrammetry and Remote Sensing, pp. 342–347.
Korpela, I., Ørka, H.O., Hyyppä, J., Heikkinen, V., Tokola, T., 2010a. Range and AGC normalization in airborne discrete-return LiDAR intensity data for forest canopies. ISPRS J. Photogramm. Remote Sens. 65, 369–379.
Korpela, I., Ørka, H.O., Maltamo, M., Tokola, T., Hyyppä, J., 2010b. Tree species classification using airborne LiDAR–effects of stand and tree parameters, downsizing of training set, intensity normalization, and sensor type. Silva Fennica 44, 319–339.
Lambert, M.C., Ung, C.H., Raulier, F., 2005. Canadian national tree aboveground biomass equations. Can. J. For. Res. 35, 1996–2018.
Leckie, D.G., Gillis, M.D., Gougeon, F., Lodin, M., Wakelin, J., Yuan, X., 1998. Computer-assisted photointerpretation aids to forest inventory mapping: some possible approaches. In: Proceedings of the International Forum on Automated Interpretation of High Spatial Resolution Digital Imagery for Forestry, pp. 10–12.
Li, J., Hu, B., Noland, T.L., 2013. Classification of tree species based on structural features derived from high density LiDAR data. Agric. For. Meteorol. 171, 104–114.
Liaw, A., Wiener, M., 2002. Classification and regression by randomForest. R News 2, 18–22.
Lin, Y., Hyyppä, J., 2016. A comprehensive but efficient framework of proposing and validating feature parameters from airborne LiDAR data for tree species classification. Int. J. Appl. Earth Obs. Geoinf. 46, 45–55.
Matikainen, L., Hyyppa, J., Litkey, P., 2016. Multispectral airborne laser scanning for automated map updating. In: Halounova, L., Bredif, M., Pajdla, T., Oude Elberink, S., Safar, V., Skaloud, J., Rottensteiner, F., Stilla, U., Limpouch, A., Schindler, K., Mayer, H., Mallet, C. (Eds.), 23rd International Archives of the Photogrammetry, Remote Sensing and Spatial Information Sciences Congress, ISPRS 2016. International Society for Photogrammetry and Remote Sensing, pp. 323–330.
Morsdorf, F., Nichol, C., Malthus, T., Woodhouse, I.H., 2009. Assessing forest structural and physiological information content of multi-spectral LiDAR waveforms by radiative transfer modelling. Remote Sens. Environ. 113, 2152–2163.
Morsy, S., Shaker, A., El-Rabbany, A., LaRocque, P.E., 2016. Airborne multispectral LiDAR data for land-cover classification and land/water mapping using different spectral indexes. ISPRS Ann. Photogramm. Remote Sens. Spat. Inf. Sci. III-3, 217–224.
Nevalainen, O., Hakala, T., Suomalainen, J., Mäkipää, R., Peltoniemi, M., Krooks, A., Kaasalainen, S., 2014. Fast and nondestructive method for leaf level chlorophyll estimation using hyperspectral LiDAR. Agric. For. Meteorol. 198–199, 250–258.
Ørka, H.O., Næsset, E., Bollandsås, O.M., 2009. Classifying species of individual trees by intensity and structure features derived from airborne laser scanner data. Remote Sens. Environ. 113, 1163–1174.
Ørka, H.O., Gobakken, T., Næsset, E., Ene, L., Lien, V., 2012. Simultaneously acquired airborne laser scanning and multispectral imagery for individual tree species identification. Can. J. Remote. Sens. 38, 125–138.
Persson, Å., Holmgren, J., Söderman, U., Olsson, H., 2004. Tree species classification of individual trees in Sweden by combining high resolution laser data with high resolution near-infrared digital images. Int. Arch. Photogramm. Remote. Sens. Spat. Inf. Sci. 36, 204–207.
R Core Team, 2015. R: A language and environment for statistical computing. R Foundation for Statistical Computing, Vienna, Austria.
Regional Municipality of York, 2010. York regional forest management plan 1998–2018, Summary March 2010. www.york.ca, Accessed date: 15 September 2017.
Roncat, A., Briese, C., Jansa, J., Pfeifer, N., 2014. Radiometrically calibrated features of full-waveform lidar point clouds based on statistical moments. IEEE Geosci. Remote Sens. Lett. 11, 549–553.
St-Onge, B., Budei, B.C., 2015. Individual tree species identification using the multispectral return intensities of the Optech Titan LiDAR system. In: Durrieu, S., Véga, C. (Eds.), Proceedings of SilviLaser 2015, pp. 71–73 (La Grande Motte, France).
St-Onge, B., Audet, F.-A., Bégin, J., 2015. Characterizing the height structure and composition of a boreal forest using an individual tree crown approach applied to photogrammetric point clouds. Forests 6, 3899.
Tompalski, P., Coops, N.C., White, J.C., Wulder, M.A., 2014. Simulating the impacts of error in species and height upon tree volume derived from airborne laser scanning data. For. Ecol. Manag. 327, 167–177.
Ustin, S.L., Gitelson, A.A., Jacquemoud, S., Schaepman, M., Asner, G.P., Gamon, J.A., Zarco-Tejada, P., 2009. Retrieval of foliar information about plant pigment systems from high resolution spectroscopy. Remote Sens. Environ. 113, S67–S77.
Vastaranta, M., Saarinen, N., Kankare, V., Holopainen, M., Kaartinen, H., Hyyppä, J., Hyyppä, H., 2014. Multisource single-tree inventory in the prediction of tree quality variables and logging recoveries. Remote Sens. 6, 3475–3491.
Vaughn, N.R., Moskal, L.M., Turnblom, E.C., 2012. Tree species detection accuracies using discrete point lidar and airborne waveform lidar. Remote Sens. 4, 377–403.
Vauhkonen, J., Tokola, T., Packalén, P., Maltamo, M., 2009. Identification of Scandinavian commercial species of individual trees from airborne laser scanning data using alpha shape metrics. For. Sci. 55, 37–47.
Vauhkonen, J., Korpela, I., Maltamo, M., Tokola, T., 2010. Imputation of single-tree attributes using airborne laser scanning-based height, intensity, and alpha shape metrics. Remote Sens. Environ. 114, 1263–1276.
Vauhkonen, J., Hakala, T., Suomalainen, J., Kaasalainen, S., Nevalainen, O., Vastaranta, M., Holopainen, M., Hyyppä, J., 2013. Classification of spruce and pine trees using active hyperspectral LiDAR. IEEE Geosci. Remote Sens. Lett. 10, 1138–1141.
Vega, C., Hamrouni, A., El Mokhtari, S., Morel, J., Bock, J., Renaud, J.P., Bouvier, M., Durrieu, S., 2014. PTrees: A point-based approach to forest tree extraction from lidar data. Int. J. Appl. Earth Obs. Geoinf. 33, 98–108.
Wagner, W., Ullrich, A., Ducic, V., Melzer, T., Studnicka, N., 2006. Gaussian decomposition and calibration of a novel small-footprint full-waveform digitising airborne laser scanner. ISPRS J. Photogramm. Remote Sens. 60, 100–112.
Wang, C.K., Tseng, Y.H., Chu, H.J., 2013. Airborne dual-wavelength LiDAR data for classifying land cover. Remote Sens. 6, 700–715.
Wei, G., Shalei, S., Bo, Z., Shuo, S., Faquan, L., Xuewu, C., 2012. Multi-wavelength canopy LiDAR for remote sensing of vegetation: design and system performance. ISPRS J. Photogramm. Remote Sens. 69, 1–9.
Wichmann, V., Bremer, M., Lindenberger, J., Rutzinger, M., Georges, C., Petrini-Monteferri, F., 2015. Evaluating the potential of multispectral airborne LiDAR for topographic mapping and land cover classification. ISPRS Ann. Photogramm. Remote Sens. Spat. Inf. Sci. II-3/W5, 113–119.
Woodhouse, I.H., Nichol, C., Sinclair, P., Jack, J., Morsdorf, F., Malthus, T.J., Patenaude, G., 2011. A multispectral canopy LiDAR demonstrator project. IEEE Geosci. Remote Sens. Lett. 8, 839–843.
Wright, I.J., Reich, P.B., Westoby, M., Ackerly, D.D., Baruch, Z., Bongers, F., Cavender-Bares, J., Chapin, T., Cornellssen, J.H.C., Diemer, M., Flexas, J., Garnier, E., Groom, P.K., Gulias, J., Hikosaka, K., Lamont, B.B., Lee, T., Lee, W., Lusk, C., Midgley, J.J., Navas, M.L., Niinemets, Ü., Oleksyn, J., Osada, H., Poorter, H., Pool, P., Prior, L.,

Pyankov, V.I., Roumet, C., Thomas, S.C., Tjoelker, M.G., Veneklaas, E.J., Villar, R., 2004. The worldwide leaf economics spectrum. Nature 428, 821–827.

Yan, W.Y., Shaker, A., 2014. Radiometric correction and normalization of airborne LiDAR intensity data for improving land-cover classification. IEEE Trans. Geosci. Remote Sens. 52, 7658–7673.

Yu, X., Litkey, P., Hyyppä, J., Holopainen, M., Vastaranta, M., 2014. Assessment of low density full-waveform airborne laser scanning for individual tree detection and tree species classification. Forests 5, 1011–1031.

Yu, X., Hyyppä, J., Litkey, P., Kaartinen, H., Vastaranta, M., Holopainen, M., 2017. Single-sensor solution to tree species classification using multispectral airborne laser scanning. Remote Sens. 9, 108.

Zou, X., Zhao, G., Li, J., Yang, Y., Fang, Y., 2016. 3D land cover classification based on multispectral lidar point clouds. In: 23rd International Archives of the Photogrammetry, Remote Sensing and Spatial Information Sciences Congress, ISPRS 2016. International Society for Photogrammetry and Remote Sensing, pp. 741–747.